Supplementary Information

for

Bio-inspired Cilia Array as the Dielectric Layer for Flexible Capacitive Pressure Sensor with High Sensitivity and Broad Detection Range

Qian Zhou,[a] Bing Ji,[a] Yuzhang Wei,[b] Bin Hu,[c] Yibo Gao,[d] Qingsong Xu,[b] Jun Zhou,[c] and Bingpu Zhou[a,]*

[a]*Joint Key Laboratory of the Ministry of Education, Institute of Applied Physics and Materials Engineering, University of Macau, Avenida da Universidade, Taipa, Macau, China*

[b]*Department of Electromechanical Engineering, Faculty of Science and Technology, University of Macau, Avenida da Universidade, Taipa, Macau, China*

[c]*Wuhan National Laboratory for Optoelectronics, Huazhong University of Science and Technology, Wuhan 430074, China*

[d]*Shenzhen Shineway Hi-Tech Corporation, Shenzhen 518112, China*

Keywords: Electronic skin, pressure sensor, cilia array, carbonyl iron particle, Polydimethylsiloxane.

Corresponding Author

Bingpu Zhou, Email: bpzhou@um.edu.mo. Fax: +853-88222426. Tel: +853-88224196.

Section S1: COMSOL simulation model

The model was established in a three-dimensional structure using COMSOL Multiphysics software. The Solid Mechanics module was selected to calculate both the stress and deformation, with the governing equation $\nabla \cdot S + Fv = 0$. In the equation, Fv is the volume force vector and $S = C : \varepsilon$, where $C = C\,(E,v)$ is a parameter of materials related to the Yong's modulus E and the Poisson's ratio v, and $\varepsilon = \frac{1}{2}[(\nabla u)^T + \nabla u]$ is the strain related to the displacement vector $\boldsymbol{u}$. The model structure was established with approximately the same size and materials used in the experiments. To evaluate the compressibility of the cilia structure, the micro pillar array was built with the diameter and height of pillars in accordance with the bottom diameter and height of the cilia. By applying vertical and parallel pressures, the stress and displacement of both the micro pillar array and micro cilia array were studied and compared. The localized stress and more obvious displacement of cilia structure reflect the better compressibility thanks to the cone-shaped structure, which promises the high sensitivity of sensor based on the cilia structure.

Section S2: Comparison of MCA and solid dielectric layer on the sensor sensitivity

For simplicity, we take the cilia dielectric layer as a mixture of the PDMS/CIP cilia and air. To start with, we have the overall dielectric constant of the MCA layer is determined by

$$\varepsilon_c = f_{cilia} \cdot \varepsilon_{pc} + (1 - f_{cilia}) \cdot \varepsilon_a$$

where f_{cilia} is the volume fraction of the cilia, ε_{pc} and ε_a are the dielectric constant of PDMS/CIP and air, respectively. Normally, the value of ε_{pc} is larger than that of ε_a. Similarly, for the dielectric constant of the solid PDMS/CIP layer, the value of ε_{solid} is $\varepsilon_{solid} = \varepsilon_{pc} > \varepsilon_c$. Under the same initial separation (d_0) between the two electrodes, the initial capacitance per unit area of the pressure sensors can be determined by

$$C_{0,\,solid} = \frac{\varepsilon_{solid}}{d_0},\quad C_{0,\,c} = \frac{\varepsilon_c}{d_0}$$

Initially with the same separation (d_0), we have $C_{0,c} < C_{0,\,solid}$. Under a specific pressure (P), we

consider that the separation of the electrodes has been reduced to d'_{solid} and d'_c, where $d'_{solid} > d'_c$ owning to the better compressibility of MCA as shown in the simulation result. Simultaneously, the dielectric constant of the solid dielectric layer remains unchanged as ε_{pc}, while that of the MCA dielectric layer has been changed to ε'_c ($\varepsilon'_c > \varepsilon_c$). The sensing sensitivity can thus be determined as

$$S_{solid} = \frac{\frac{\Delta C_{solid}}{C_{0,solid}}}{P} = \frac{\frac{\varepsilon_{solid}/d'_{solid}}{\varepsilon_{solid}/d_0} - 1}{P} = \frac{\frac{d_0}{d'_{solid}} - 1}{P}$$

and

$$S_c = \frac{\frac{\Delta C_c}{C_{0,c}}}{P} = \frac{\frac{\varepsilon'_c/d'_c}{\varepsilon_c/d_0} - 1}{P} = \frac{\frac{\varepsilon'_c \cdot d_0}{\varepsilon_c \cdot d'_c} - 1}{P} > \frac{\frac{\varepsilon_c \cdot d_0}{\varepsilon_c \cdot d'_{solid}} - 1}{P} = \frac{\frac{d_0}{d'_{solid}} - 1}{P} = S_{solid}$$

The results above confirm that both of the separation between the two electrodes and the variation of the dielectric constant from the MCA layer can be positive to the improvement of the sensitivity.

Section S3: Effect of the cilia volume fraction (5:4@500 and 5:3@500)

Followed with the analysis in **Section S2**, the air was completely removed from the dielectric layer of MCA with the continuous compression, leading to the final dielectric constant as of

$$\varepsilon'_c = \varepsilon_{pc}$$

The variation of the dielectric constant for this case can be defined as

$$\Delta\varepsilon = \varepsilon'_c - \varepsilon_c = \varepsilon_{pc} - \left[f_{cilia} \cdot \varepsilon_{pc} + (1 - f_{cilia}) \cdot \varepsilon_a\right] = (1 - f_{cilia}) \cdot (\varepsilon_{pc} + \varepsilon_a)$$

From the above formula, we can observe that a smaller value of f_{cilia} can result in a higher $\Delta\varepsilon$, and thus more positive to the variation of the dielectric constant and the sensor sensitivity.

Section S4: Comparison of the underlying substrate

For capacitors connected in series, the equivalent capacitance (C_{eq}) can be explained as,

$$\frac{1}{C_{eq}} = \sum_{j=1}^{n} \frac{1}{C_j}$$

where n denotes the number of the individual capacitor, and C_j is the capacitance of each capacitor in series. Based on the schematic in **Figure 3c**, we thus have the capacitance

$$\frac{1}{C_{eq}} = \frac{1}{C_{cilia}} + \frac{1}{C_{substrate}}$$

where C_{cilia} and $C_{substrate}$ denote the capacitance component from the cilia layer and the substrate, respectively. For the substrate with dielectric constant of ε_s and thickness of d_s, we have the capacitance of the underlying substrate per unit area, $C_{substrate} = \frac{\varepsilon_s}{d_s}$. For the cilia layer with dielectric constant of ε_c and height of d_c, we have the capacitance of the cilia dielectric layer per unit area, $C_{cilia} = \frac{\varepsilon_c}{d_c}$. It should be noted here that the value of ε_c is the combinational effect from the dielectric constant of air (ε_a) and that of the PDMS/CIP cilia (ε_{pc}). We thus have

$$C_{eq} = \frac{1}{\frac{1}{C_{cilia}} + \frac{1}{C_{substrate}}} = \frac{\varepsilon_s}{\frac{d_c}{\varepsilon_c} \cdot \varepsilon_s + d_s}$$

With the continuous pressing, the height of the compressed cilia layer has been changed to $d_c^{'}$ and corresponding dielectric constant has been changed to $\varepsilon_c^{'}$. Compared with the obvious variation of Δd_c, the thickness variation of the underlying substrate can be ignored (Δd_s=0, $d_s^{'} = d_s$). We thus have the relative change of the capacitance as

$$\frac{\Delta C}{C} = \frac{C_{eq}^{'} - C_{eq}}{C_{eq}} = \frac{\varepsilon_s \cdot \left(\frac{d_c}{\varepsilon_c} - \frac{d_c^{'}}{\varepsilon_c^{'}} \right)}{\frac{d_c^{'}}{\varepsilon_c^{'}} \cdot \varepsilon_s + d_s}$$

From the formula, we can conclude with reduced thickness of the substrate, the pressure sensitivity can be improved under the high pressure regime as shown in **Figure 3f**.

Reference

1. S. R. A. Ruth, L. Beker, H. Tran, V. R. Feig, N. Matsuhisa and Z. Bao, *Adv. Funct. Mater.*, 2019, 1903100. DOI: 10.1002/adfm.201903100.

2. D. Kwon, T. I. Lee, J. Shim, S. Ryu, M. S. Kim, S. Kim, T. S. Kim and I. Park, *ACS Appl. Mater. Interfaces*, 2016, **8**, 16922-16931.

3. Y. Luo, J. Shao, S. Chen, X. Chen, H. Tian, X. Li, L. Wang, D. Wang and B. Lu, *ACS Appl. Mater. Interfaces*, 2019, **11**, 17796-17803.

4. X. Shuai, P. Zhu, W. Zeng, Y. Hu, X. Liang, Y. Zhang, R. Sun and C. P. Wong, *ACS Appl. Mater. Interfaces*, 2017, **9**, 26314-26324.

5. Y. Wan, Z. Qiu, J. Huang, J. Yang, Q. Wang, P. Lu, J. Yang, J. Zhang, S. Huang, Z. Wu and C. F. Guo, *Small*, 2018, **14**, 1801657.

6. Z. He, W. Chen, B. Liang, C. Liu, L. Yang, D. Lu, Z. Mo, H. Zhu, Z. Tang and X. Gui, *ACS Appl. Mater. Interfaces*, 2018, **10**, 12816-12823.

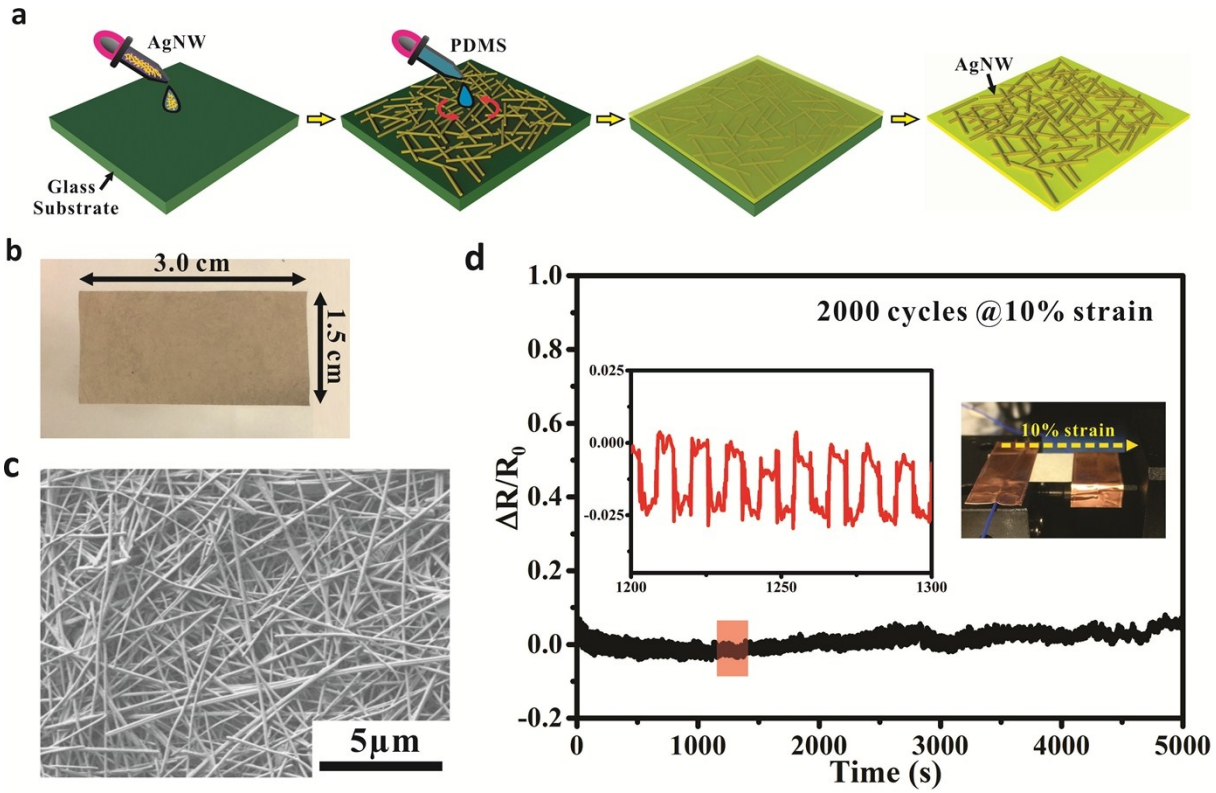

Figure S1. a) Schematic of the preparation process of AgNWs/PDMS electrode. b) Optical images of a typical AgNWs/PDMS electrode with dimension of 3.0 cm×1.5 cm. c) SEM images of the as-prepared

AgNWs. d) Stability of the electric conductivity of the AgNWs/PDMS electrode via cyclic stretching for 2000 cycles.

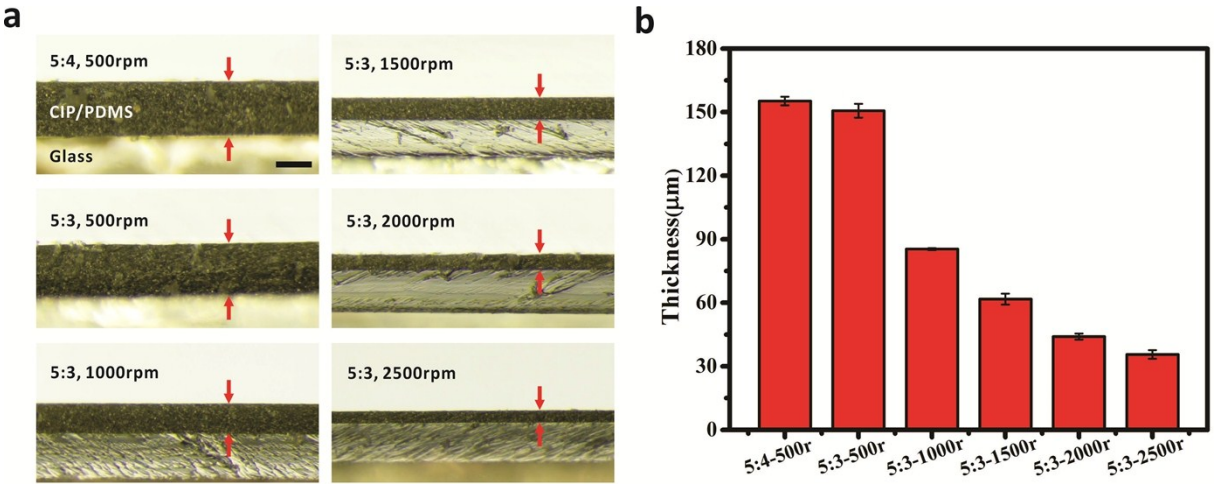

Figure S2. a) The side-view optical images of PDMS/CIP membranes related to different mass ratios and spin-coating speeds. Scale bars: 100 μm for all optical images. b**)** Typical dependence of the membrane thickness based on the mass ratios and spin-coating speeds.

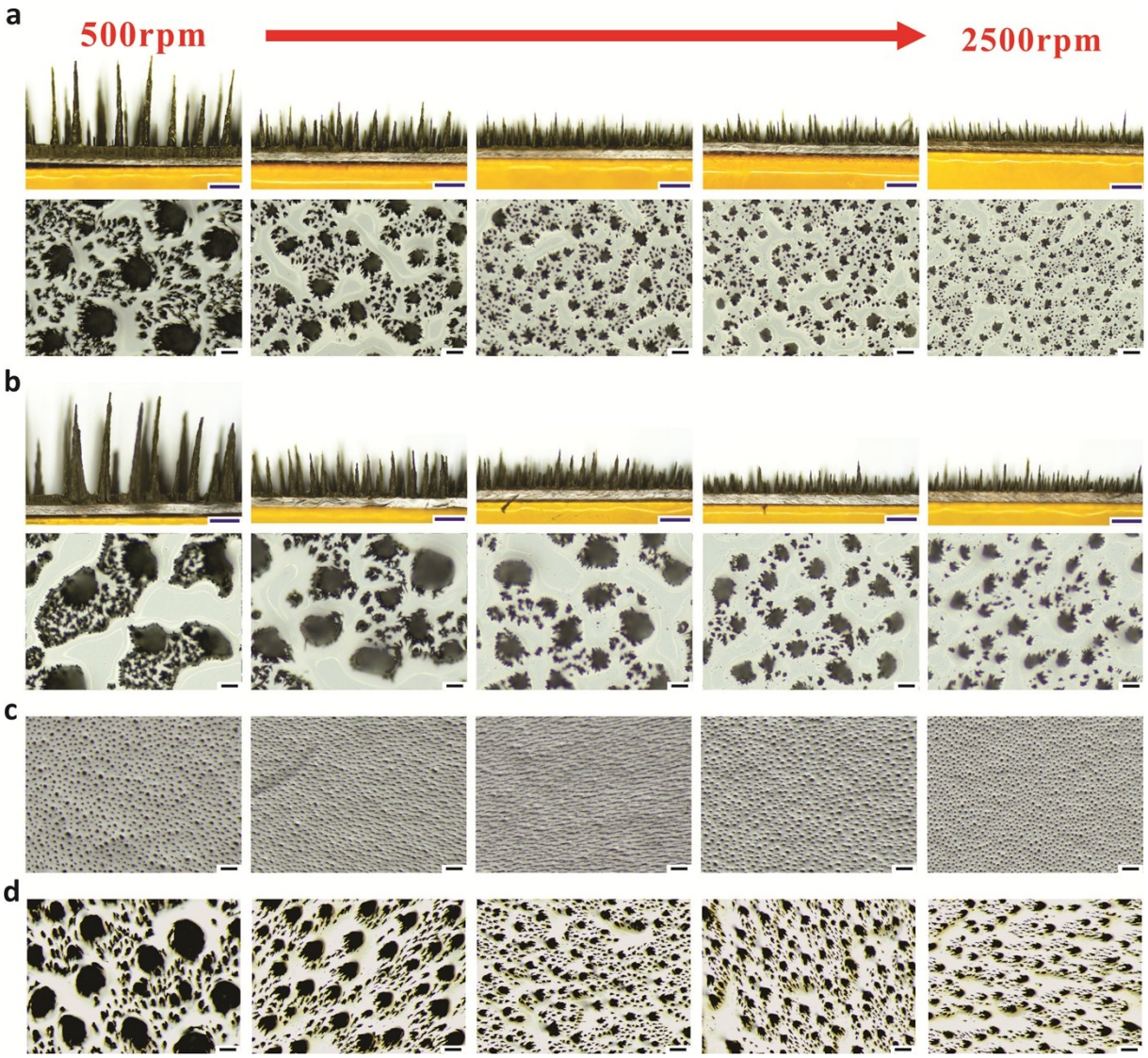

Figure S3. Typical top-view and side-view optical images of the MCA with different spin-coating speeds and PDMS/CIP mass ratios, a) 5:3; b) 5:4; c) 5:0.5; d) 5:2. Scale bars: 500 μm and 100 μm for side-view and top-view optical images, respectively.

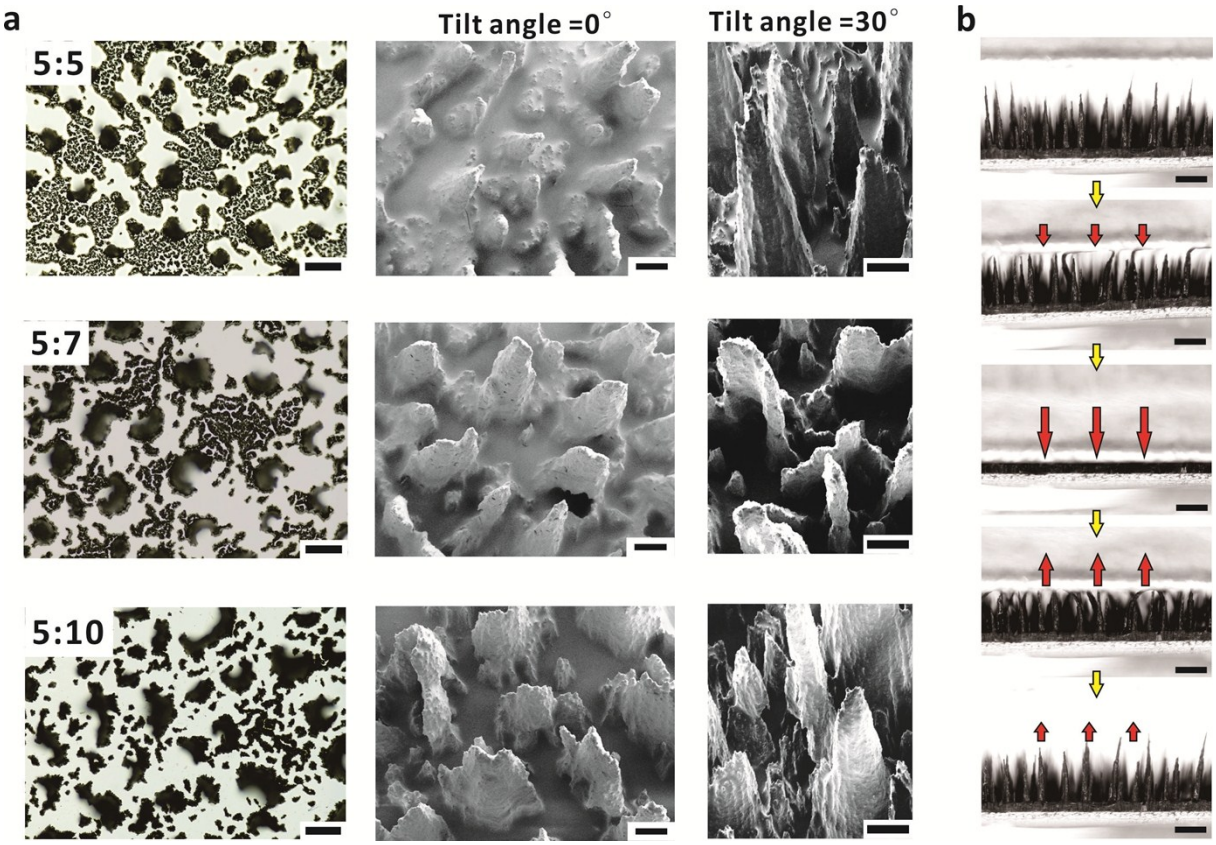

Figure S4. a) Optical images and SEM images (tilt angle of 0° and 30°) of the as-prepared cilia structures based on different mass ratios of PDMS/CIP. b) Side-view optical images of the loading and unloading process of the MCA (5:3@500). Scale bars: 500 μm and 200 μm for optical images and SEM images, respectively.

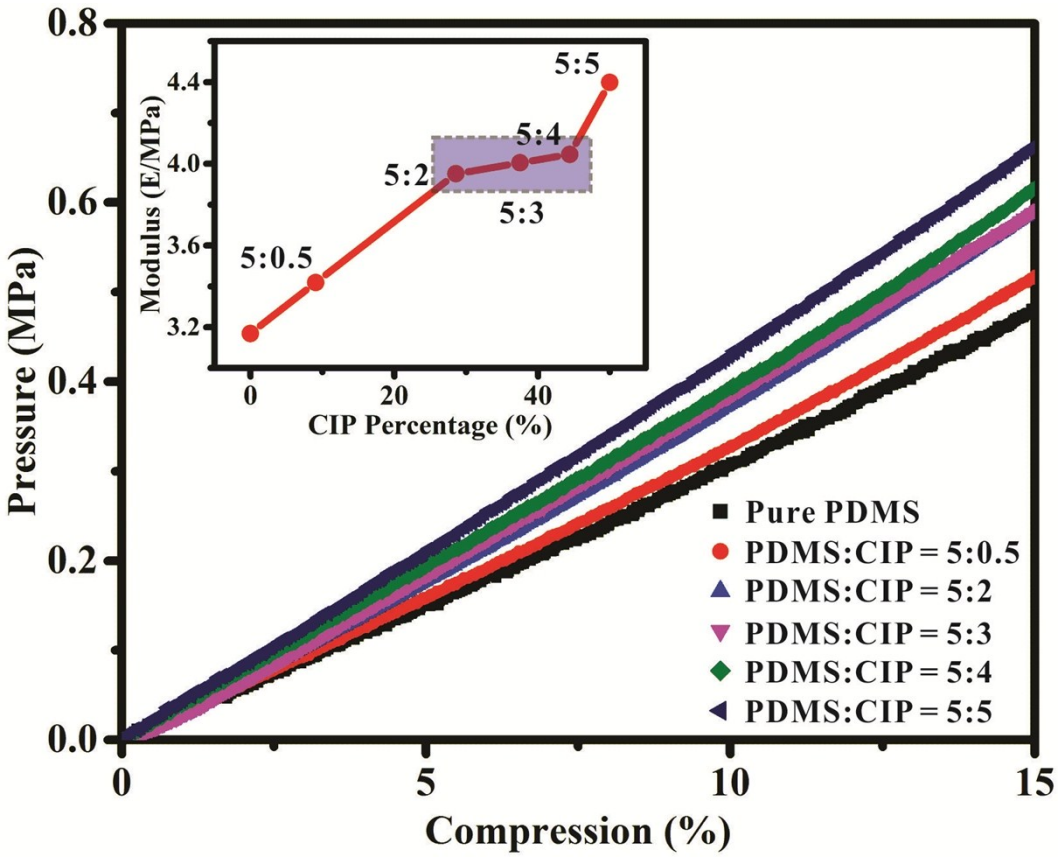

Figure S5. Elastic modulus of PDMS/CIP membranes with different mass ratios.

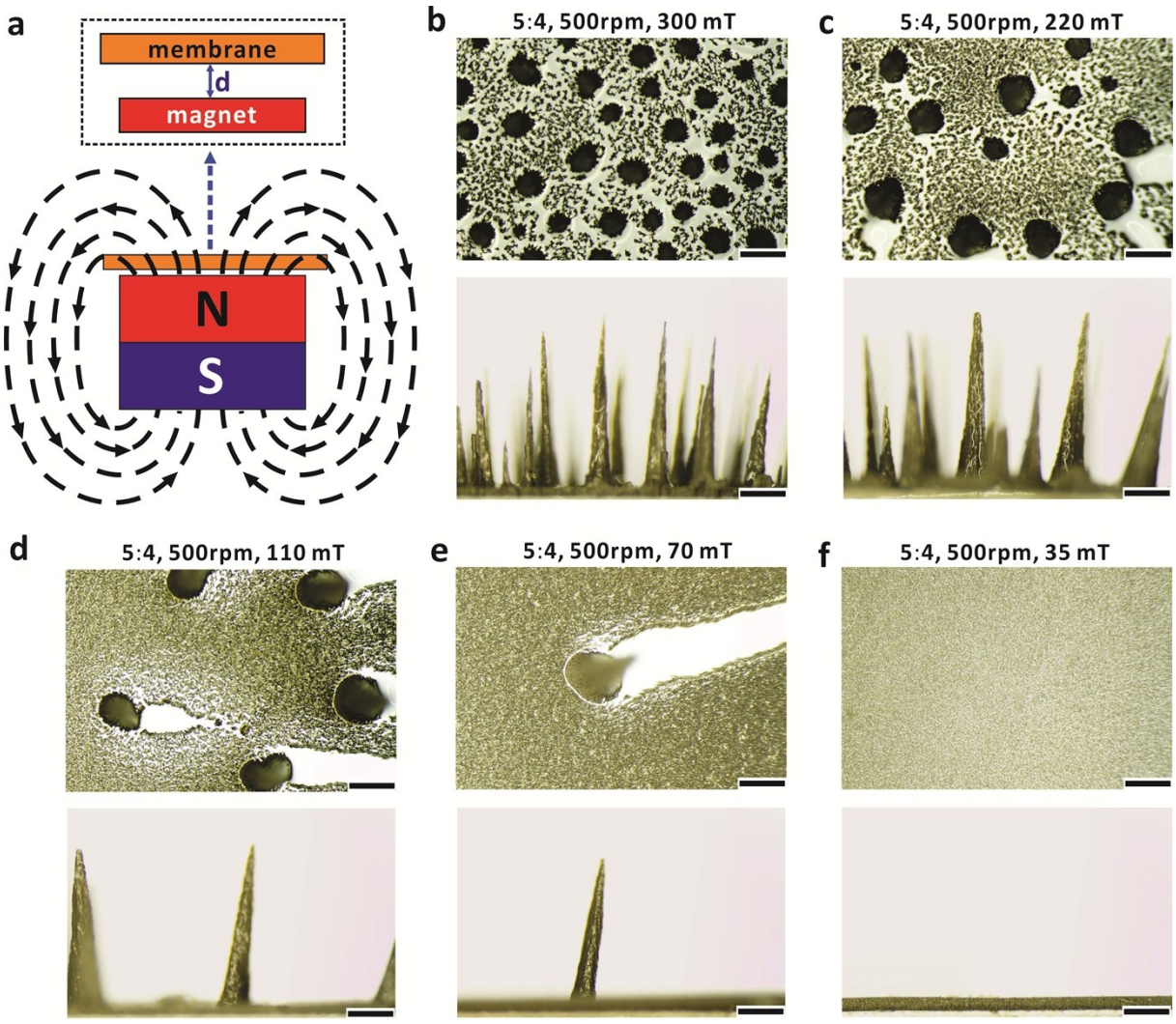

Figure S6. The morphology and arrangement of MCA with respect to the magnetic fields by placing the PDMS/CIP membrane with different distance from the surface of a permanent magnet. Corresponding magnetic fields were measured via a commercial magnetic probe. Scale bars: 500 μm for all optical images.

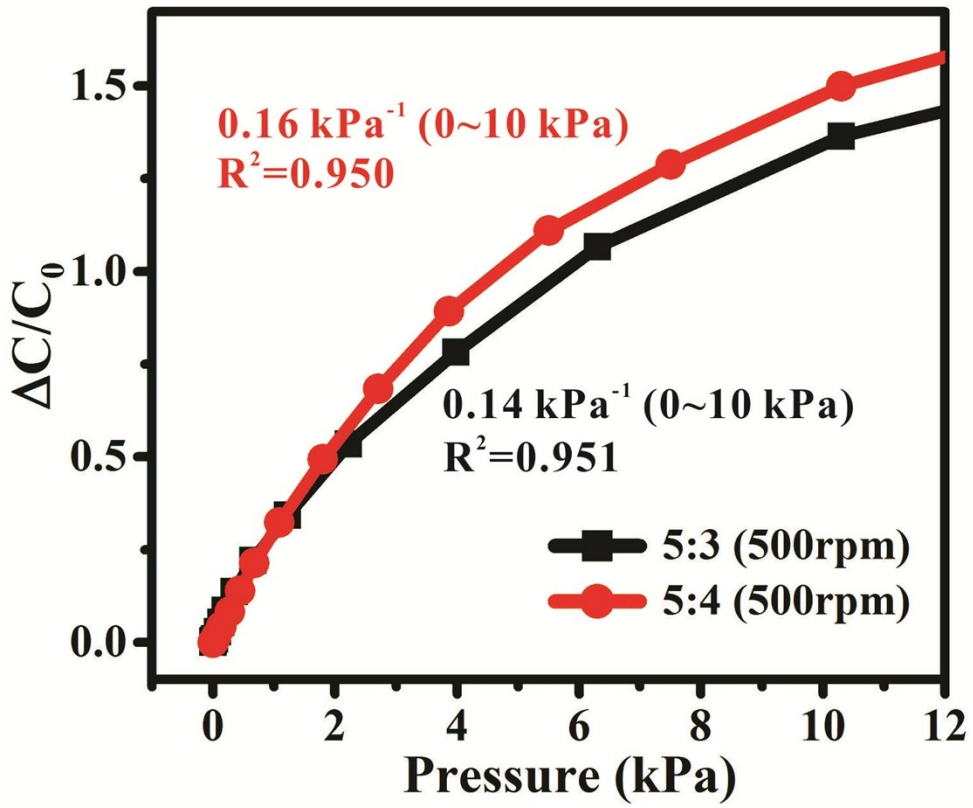

Figure S7. Comparison of $\Delta C/C_0$ as a function of applied pressure (0 - 12 kPa) with regards of different average heights of MCA prepared via 5:4@500 and 5:3@500.

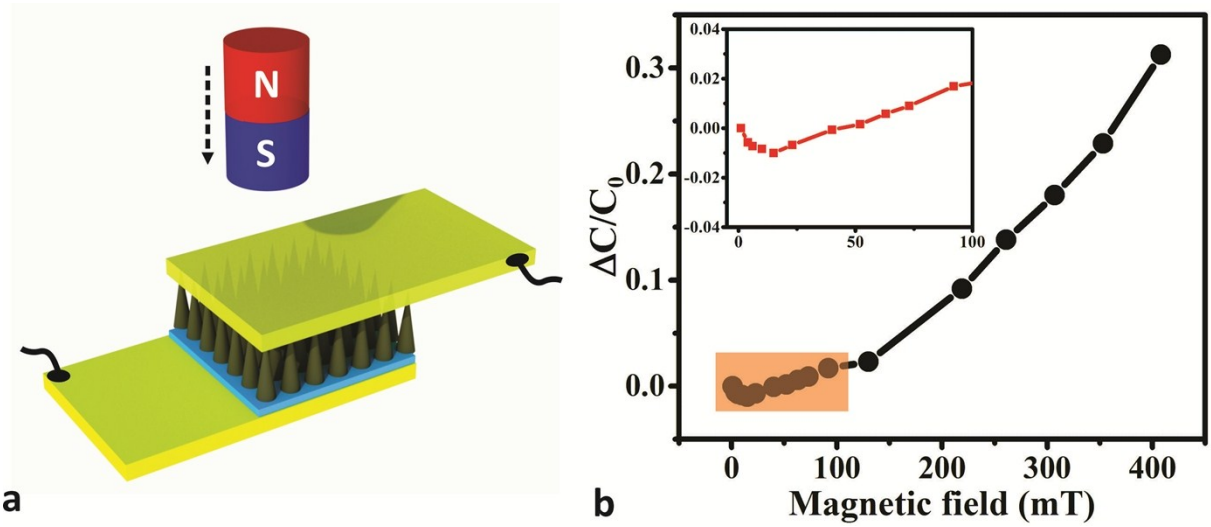

Figure S8. a) Schematic of the experimental setup to examine the capacitance response capability of the pressure sensor under different magnitudes of the magnetic field from a portable permanent magnet. b) Related response curve of the capacitance variation when the device was exposed to different magnetic fields.

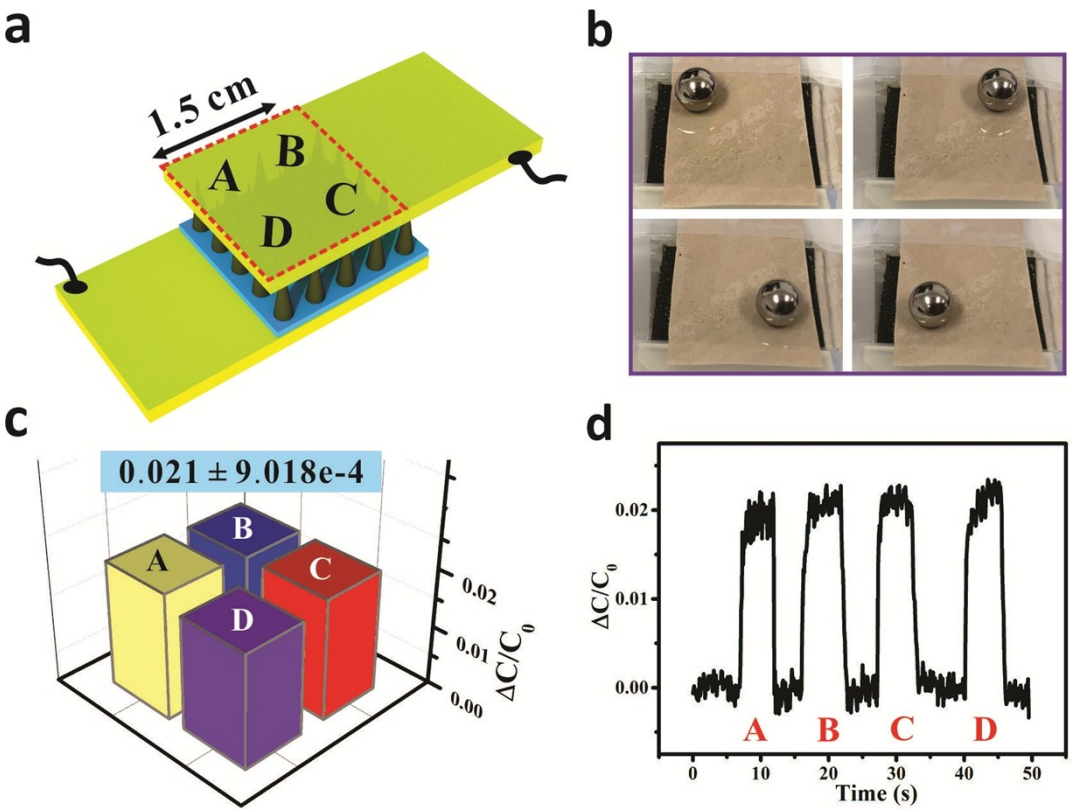

Figure S9. a) Schematic of the uniformity test of the pressure sensor. b) Setup of the uniformity test via placing the steel ball to four different regions. c) Related capacitance change of the four regions after loading the steel ball. d) Detailed data of the uniformity test from four different regions.

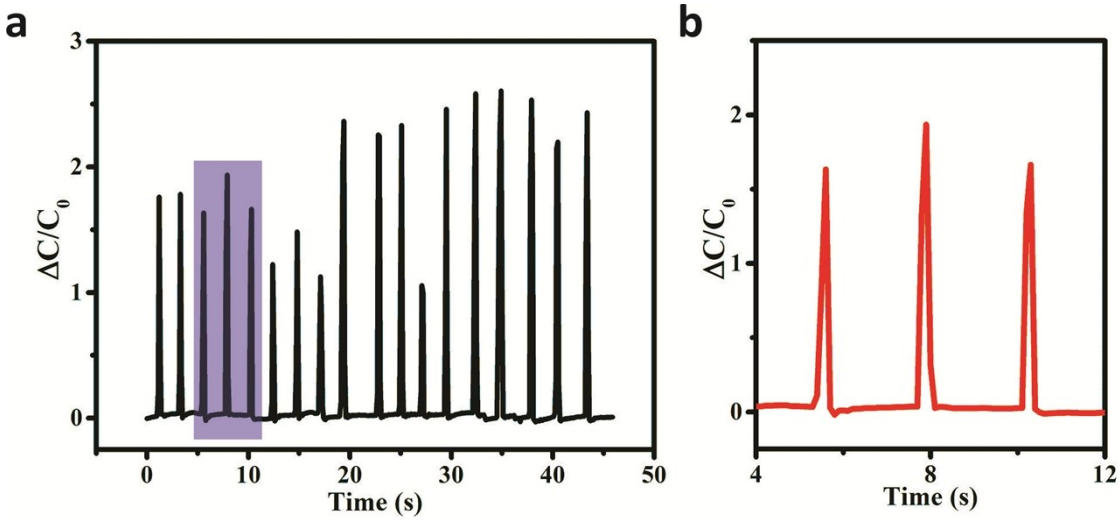

Figure S10. Real-time response test of the pressure sensor via swift finger bending.

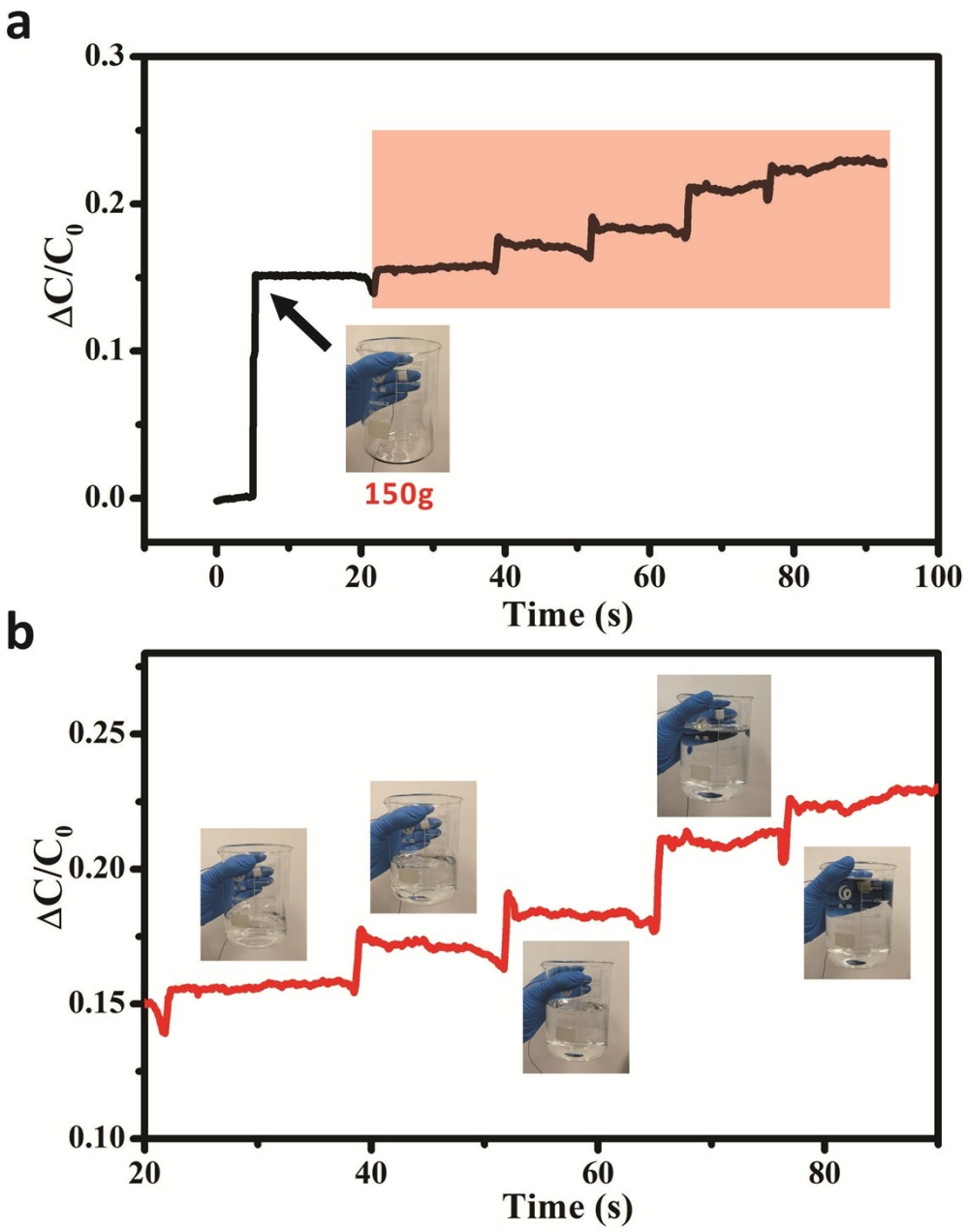

Figure S11. Real-time capacitance variations with regards to capturing the glass beaker of different weights through adding water.